PNAS RESEARCH ARTICLE | EARTH, ATMOSPHERIC, AND PLANETARY SCIENCES

Structural and electronic transformations of $GeSe_2$ glass under high pressures studied by X-ray absorption spectroscopy

Emin Mijit[a,b,1], Murat Durandurdu[c], João Elias F. S. Rodrigues[b], Angela Trapananti[a], S. Javad Rezvani[a], Angelika Dorothea Rosa[b], Olivier Mathon[b], Tetsuo Irifune[d], and Andrea Di Cicco[a,1]

Edited by Alexandra Navrotsky, Arizona State University, Tempe, AZ; received October 30, 2023; accepted February 20, 2024

Pressure-induced transformations in an archetypal chalcogenide glass ($GeSe_2$) have been investigated up to 157 GPa by X-ray absorption spectroscopy (XAS) and molecular dynamics (MD) simulations. Ge and Se K-edge XAS data allowed simultaneous tracking of the correlated local structural and electronic changes at both Ge and Se sites. Thanks to the simultaneous analysis of extended X-ray absorption fine structure (EXAFS) signals of both edges, reliable quantitative information about the evolution of the first neighbor Ge-Se distribution could be obtained. It also allowed to account for contributions of the Ge-Ge and Se-Se bond distributions (chemical disorder). The low-density to high-density amorphous-amorphous transformation was found to occur within 10 to 30 GPa pressure range, but the conversion from tetrahedral to octahedral coordination of the Ge sites is completed above ∼ 80 GPa. No convincing evidence of another high-density amorphous state with coordination number larger than six was found within the investigated pressure range. The number of short Ge-Ge and Se-Se "wrong" bonds was found to increase upon pressurization. Experimental XAS results are confirmed by MD simulations, indicating the increase of chemical disorder under high pressure.

polyamorphism | high pressure | X-ray absorption spectroscopy | chemical disorder

Significance

Structure of simple tetrahedral glasses under high pressures, particularly near or beyond Mbar range has been intensely debated, but remained elusive. Behavior of network forming glasses with "wrong-bonds" under such extreme conditions is even more poorly understood due to the extra (chemical) disorder within these systems. Here, properties of an archetypal chalcogenide glass ($GeSe_2$) have been studied using X-ray absorption spectroscopy up to 157 GPa. Pressure-induced changes in the local structure, electronic configuration, and chemical disorder related to both Ge and Se sites have been probed and described quantitatively. Results show a considerable increase in the chemical disorder. However, no convincing evidence of an amorphous state with coordination numbers larger than six was observed within the investigated pressure range.

Apart from the fundamental questions related to the nature of amorphous-amorphous transformation (polyamorphism), understanding the atomic scale structure and densification process of network forming glasses under high pressure (HP) is a matter of significant importance in different fields of research, ranging from materials to Earth and planetary sciences. For instance, comprehension of the pressure-induced local structural changes and densification mechanism in a simple network forming glass such as amorphous SiO_2 has implications for understanding the behavior and characteristics of silicate melts in the Earth's deep interior (1–5). On that account, polyamorphism has been extensively investigated over the last few decades, mostly on simple model systems with directional bonding and open local structures (5–12).

Even though the detailed nature of most of the high-pressure amorphous-amorphous transformations is still a matter of debate, some progress has been made in understanding the behavior polyamorphism in prototypical network forming glasses. A consensus has been reached regarding the phenomenological aspects, such as the gradual increase of nearest neighbor coordination numbers (CNs) from fourfold to fivefold or sixfold along the densification from low-density amorphous (LDA) to high-density amorphous (HDA) state (5–8), which typically takes place at moderate high pressures (within 15 to 50 GPa). According to some recent studies on oxide glasses, the pressure-induced increase of the CNs of the network forming structural motifs, and thus polyamorphic transformations can be also explained in terms of oxygen packing efficiencies (13–15). Nevertheless, further densification processes of these systems beyond the HDA state with CN $\approx$ 6 remain a matter of debate. Experimental efforts in recent years have aimed to investigate further structural changes in network forming glasses beyond the HDA state, extending the pressure ranges up to 1 Mbar or even higher. Several studies on archetypal SiO_2 and GeO_2 glasses have discussed the possibility of a second stage of densification leading to an amorphous state with $CN > 6$ (1, 2, 14–16). However, no consensus was found, as other studies suggest the persistence of octahedral coordination (CN = 6) in the same compounds within similar pressure ranges (17–19). Moreover, little attention has been given to the evolution of electronic structure and its correlation with the changes of local atomic structure (16, 19, 20).

One of the main challenges in conducting structural studies of network forming glasses under ultrahigh pressures is the limitation posed by standard structure characterization techniques like x-ray diffraction, due to weak scattering signals from tiny amorphous

Author contributions: E.M. and A.D.C. designed research; E.M., M.D., J.E.F.S.R., A.T., S.J.R., A.D.R., O.M., T.I., and A.D.C. performed research; E.M. and A.D. contributed new reagents/analytic tools; E.M. and A.D.C. analyzed data; and E.M. and A.D.C. wrote the paper.

The authors declare no competing interest.

This article is a PNAS Direct Submission.

[1]To whom correspondence may be addressed. Email: emin.mijit.17@gmail.com or andrea.dicicco@unicam.it.

This article contains supporting information online at https://www.pnas.org/lookup/suppl/doi:10.1073/pnas.2318978121/-/DCSupplemental.

Published March 27, 2024.

samples (typically in a diamond anvil cell). In addition to conventional diffraction-based techniques, X-ray absorption spectroscopy represents a powerful complementary technique to be applied for disordered systems. XAS is a direct probe of local structural correlations in the sample, without contribution from the sample environment. Thus, it is ideally suited for studying local structural changes in the glassy materials under ultrahigh pressures by EXAFS analysis. Being an element-specific technique, XAS and its features are directly related with the outer shell electronic configurations of the target atomic species, can provide complementary insight concerning the evolution of the chemical bonds and structural rearrangements. Even though XAS has been used in many cases for the studies of glassy system (such as GeO_2, $GeSe_2$, and As_2Se_3) under moderate pressures (6, 11, 21–24), its capabilities have not been exploited for studying the pressure behavior of amorphous systems under ultrahigh pressures, except rare cases of chemically complex glasses that occurred very recently (25, 26).

Similarly to oxide glasses, chalcogenide glasses also undergo densification characterized by a significant increase of CN across the LDA to HDA transformation (7, 11, 21, 23, 27–29). However, due to the presence of chemical disorder (or irregular homopolar bonds among like atoms) (7, 11, 30, 31), some differences in the pressure behavior were observed in chalcogenide glasses. In particular, few studies performed by X-ray diffraction and molecular dynamics simulations have suggested the increase of chemical disorder under pressure, and the promotion of homopolar bonds was suggested to play certain role in the formation of higher coordinated species (27, 28). Nevertheless, the evolution and influence of chemical disorder in the pressure behavior of chalcogenide glasses, especially in the context of their ultrahigh-pressure polyamorphism remain largely unexplored. Evolution of chemical disorder and its effect on the densification of chalcogenide glasses need to be confirmed and further clarified using direct and element-selective local structure probes such as EXAFS.

Here, we have investigated the pressure-induced transformations in a particular simple model system: $GeSe_2$ chalcogenide glass up to 157 GPa using the XAS measurements. Complementary molecular dynamics (MD) simulations have also been performed to assist XAS data analysis. Possibility of scanning both Ge and Se K-edges at the same pressures (thanks to the proximity of the two edges) along a single compression run allowed us to probe local structural changes of both Ge and Se sites simultaneously. Accurate EXAFS analysis could be performed on extended k-spaces using double-edge refinements in a wide pressure range. As a result, reliable structural information concerning the changes in nearest neighbor Ge-Se distribution could be achieved, tracking also the evolution of chemical disorder by including contributions of the Ge-Ge and Se-Se homopolar bonds in our EXAFS analysis. Some changes in electronic configurations (p-like empty states of Ge and Se atoms) could be monitored from the near-edge XAS. These electronic configurations are directly involved in the chemical bonding; thus, near-edge XAS features have provided valuable complementary insights into the pressure-induced band-gap closure (metallization), structural rearrangements, and evolution of the chemical disorder.

Results and Discussion

In the following paragraphs, we will present and discuss the results of XAS data analysis. We will begin by discussing the x-ray absorption near edge structure (XANES) in a dedicated subsection, followed by a comprehensive quantitative analysis of the EXAFS signals. Angular dispersive XRD data that have been measured during the compression run are reported in the (*SI Appendix*) file (*SI Appendix*, Fig. S1). No sign of crystallization has been identified from the XRD data, confirming that $GeSe_2$ glass remained amorphous within the entire pressure range (up to 157 GPa).

XANES Evolution. Due to the longer mean free path of low-energy photoelectrons and the importance of higher-order many-body multiple scattering signals, XANES features are highly sensitive to pressure-induced modifications in the three-dimensional structural topology that extend beyond the nearest coordination shell (32–35). Moreover, XAS probe the unoccupied projected electronic density of states (36), so pressure-induced changes of the electronic properties are reflected by corresponding changes in shape and positions of the XANES features.

Normalized Ge and Se *K*-edge XANES spectra collected at different pressures are presented with vertical offset in Fig. 1 *A* and *B*. For better visualizing spectral changes, we plot XANES spectra of several selected pressures with the same scale (without vertical offset) in Fig. 1 *C* and *D*. We can see that XANES features of

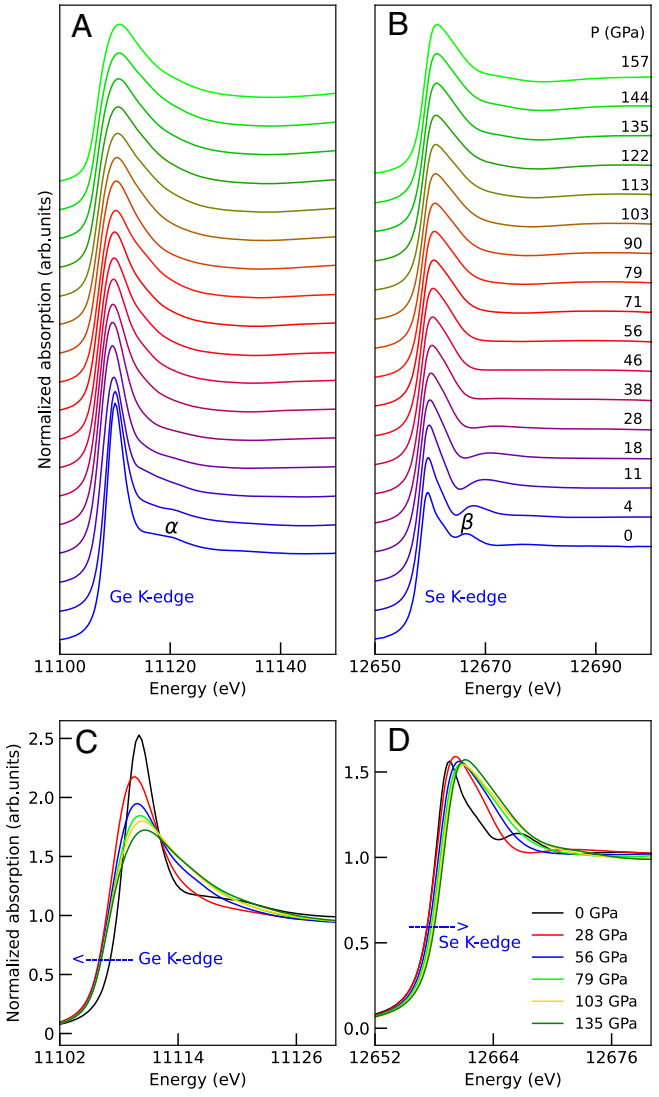

Fig. 1. Normalized Ge (*A*) and Se (*B*) *K*-edge XANES at different pressures up to 157 GPa were plotted with vertical offset. Normalized Ge (*C*) and Se (*D*) *K*-edge XANES at selected pressure points were plotted in the same scale without vertical offset.

both edges show large changes under pressure. In the Ge K-edge XANES, intensity of the weak feature just after the white line peak [labeled as α in Fig. 1*A*] decreases rapidly and changes to a slope-like feature around 11 GPa. A similar feature observed at the Se *K*-edge [labeled as β in Fig. 1*B*], is broadened and shifted to higher energies up to 11 GPa. These spectral changes are consistent with the breakdown of the intermediate range ordering and depopulation of edge-sharing tetrahedral units which were observed early (37–39) in this pressure range. These features (evolved from α and β) became weak and gradually disappeared at about 28 GPa, being associated with the rapid changes in the short and intermediate range ordering along the LDA to HDA transformation (in 10 to 30 GPa range) which will be discussed in details in the next sections.

Another significant spectral change that is readily noticeable in Fig. 1 *C* and *D* is the energy shift of the rising edges at higher pressures. For a more comprehensive evaluation, we plotted the shift of Ge and Se *K*-edge edge energies [$\Delta E_e(P) = E_e(P) - E_e(P_{1bar})$] as a function of pressure in Fig. 2, along with previously reported values from our earlier work up to 30 to 45 GPa (11, 29). Here, the edge energy E_e is determined in the standard way, by identifying the energy position of the first maximum of the first derivative spectra. As we can see from Fig. 2, both edge positions are stable around their initial values (within the error bars) in the initial compression stage up to 11 GPa. Above this pressure, however, Ge K-edge edge energy (E_e^{Ge}) shows a rapid shift to lower energies, while E_e^{Se} seem to show a little decrease but remained constant within the error bars up to $\sim$ 50 GPa. At the same time, the shift of E_e^{Ge} (ΔE_e^{Ge}) reaches -1.5 eV around 30 GPa and continue to decrease until 120 GPa but with a slower rate. Interestingly, Se *K*-edge shows a blue shift above $\sim$ 50 GPa. The ΔE_e^{Se} exceeds error bars and reaches a value of about 0.5 eV around $\sim$120 GPa. Above this pressure, both Ge and Se *K*-edges were found to be almost stable until the highest pressure attained (157 GPa). The edge shifts are obviously associated with a change in the energy position of the first unoccupied states. Interpretation of this behavior can be done similarly to the case of the transitions from semiconducting to metallic Ge (40, 41).

For pressurized $GeSe_2$ glass, the overall behavior of edge energies can be described by four different stages as indicated by the background colors of Fig. 2. The large red shift of Ge *K*-edge is consistent with the semiconducting (SMC) to metal (M) transition which is known to occur within 10 to 20 GPa range (11, 29, 42, 43). Pressure-induced metallization is also evident from the evolution of the relative reflectivity of the sample (with respect to the metallic Re gasket), which we can see from the optical images given in *SI Appendix*, Fig. S2. The sample at 27 GPa is more reflective than the initial sample, indicating a reduced or completely closed band-gap. At 100 GPa, the sample is completely opaque, and can not be distinguished from the metallic Re gasket. This implies an increased metallicity, possibly with more free electrons in the sample as also indicated by the further decrease of E_e^{Ge}. Both from the evolution of the relative reflectivity and edge energy shifts shown in Fig. 2, we can speculate that the sample at the intermediate- (20 to 100) and ultrahigh-pressure (>100 GPa) ranges may have different electronic states. On the other hand, the increase of E_e^{Se} above 40 to 50 GPa is consistent with an increase in the number of "wrong" nearly covalent Se-Se bonds at higher pressures because the Se-Se bonding will increase the effective valence of Se to higher values. Formation of Se-Se wrong bonds which is evident also from the EXAFS analysis will be discussed again in the next sections. Another important change in the XANES spectra is that the white line peak becomes more broadened and asymmetric at higher pressure above 50 GPa, being much more evident at the Ge *K*-edge. This is consistent with a broadening and delocalization of the p-like density of states after the metallization. Qualitatively speaking, large modifications of XANES spectral line shapes of both edges nonambiguously manifest substantial structural and electronic changes in the $GeSe_2$ glass under pressure.

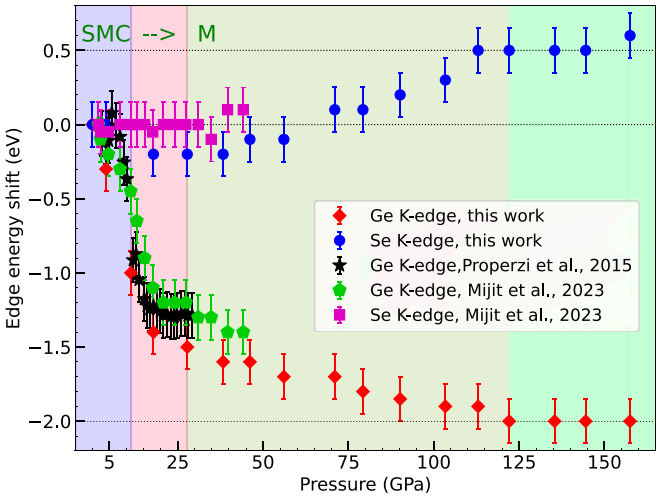

Fig. 2. Energy shifts of Ge and Se K-edges as a function of pressure.

EXAFS Analysis. EXAFS signals extracted from high-pressure XAS data have been analyzed using the GNXAS method (44–46). The Ge and Se K-edge EXAFS spectra at each pressure have been simultaneously analyzed using multiedge refinement features of the GNXAS package (47). Structural parameters considered here are those related to the short-range Ge-Se, Ge-Ge, and Se-Se atomic partial distribution functions. In this covalent glass they can be conveniently described by simple Gaussian peaks defined by average bond distances (R), variances (σ^2) and coordination numbers (CN). The most important EXAFS contribution is related to the Ge-Se distribution, while Ge-Ge and Se-Se contributions are associated with the presence of so-called "wrong" bonds between like atoms, indicating the presence of chemical disorder. Within the multiedge refining scheme, parameters related to Ge-Se bonds are constrained to be the same for both the Ge and Se K-edge fitting.

We have considered two different models for EXAFS refinements. The first model (model-1) was an assumption of negligible chemical disorder, so only Ge-Se signals at both Ge and Se K-edges were considered. Of course, for the nearest Ge-Se distribution, the CN of the Se was constrained to be half of the CN of Ge, according to the known stoichiometry. An exemplary double-edge refinement of EXAFS data (measured at $P = 56.0$ GPa) using model-1 is given in the upper panels of Fig. 3. In this figure, the $k^2\chi(k)$ signals of two edges are presented with the same vertical scale. Differences in their amplitude are mainly associated with the difference of coordination numbers and backscattering amplitudes of Ge and Se atoms. As shown in Fig. 3 *A* and *D*, calculated best-fit signals reproduce the experimental EXAFS oscillations, but there is also a visible mismatch, readily visible in the Fourier Transforms (Fig. 3 *C* and *F*). In order to improve the agreement between calculated and experimental EXAFS data, we introduced the possibility of accounting for chemical disorder (model-2), so the inclusion of additional contribution from

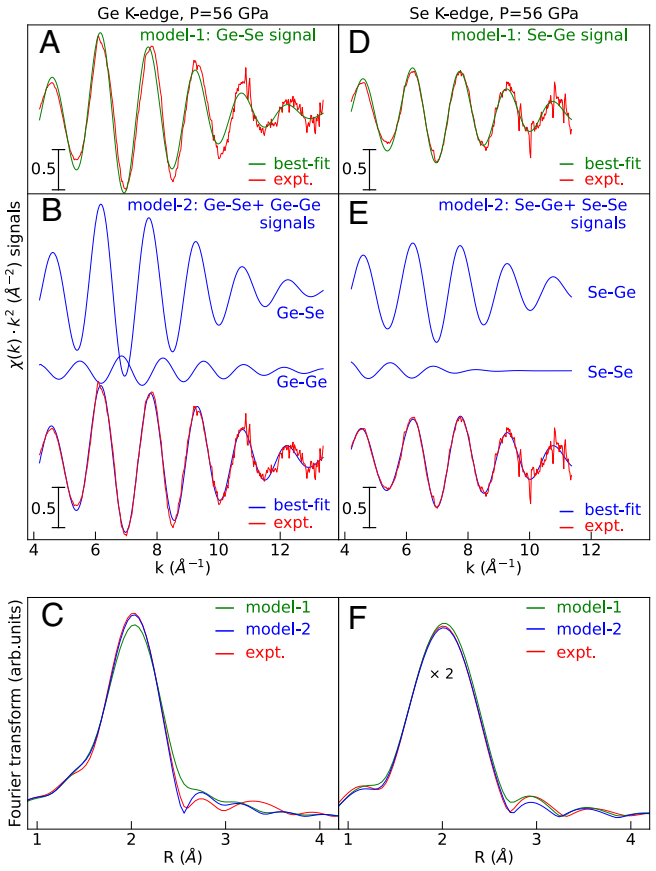

Fig. 3. (*A*) Experimental and best-fit calculated EXAFS signals at the Ge *K*-edge. Only the Ge-Se distribution (model-1) is considered in the calculated signal. (*B*) Experimental and best-fit theoretical EXAFS signals at the Ge *K*-edge. Distributions of Ge-Se and Ge-Ge distances (model-2) were considered to produce the total calculated signal. (*C*) Fourier transforms of experimental and calculated EXAFS signals reported in panels (*A*) and (*B*). (*D*) Experimental and best-fit theoretical EXAFS signals at the Se *K*-edge. Only the Se-Ge distribution (model-1) is considered in the calculated signal. (*E*) Experimental and best-fit theoretical EXAFS signals at the Se *K*-edge. Distributions of Se-Ge and Se-Se distances (model-2) were considered to produce the total calculated signal. (*F*) Fourier transforms of experimental and simulated EXAFS signals reported in panels (*D*) and (*E*). Intensity of the Fourier transforms in (F) was multiplied by two.

"wrong" Ge-Ge and Se-Se bonds. In fact, the presence of chemical disorder in $GeSe_2$ glass is well known in the literature (7, 30, 31) although detection is possible only using very accurate and low-noise data as it was done previously at ambient pressure (11). Indeed, including these extra signals was found to improve the agreement with experimental data, facilitating also a reasonable modeling of the background. As we can see from Fig. 3 *B* and *E*, experimental and best-fit calculated signals (model-2) reached a perfect agreement with the inclusion of Ge-Ge and Se-Se signals. Improvement of the refinement can be appreciated also looking at the Fourier transforms of the experimental and theoretical signals shown in Fig. 3 *C* and *F*. It's important to note that despite the scattering amplitudes and phase shifts of Ge and Se atoms are similar, inclusion and identification of Ge-Ge and Se-Se signals in the EXAFS refinement are considered reasonable based on the well-established prior knowledge (from our MD simulations and relevant literature) about the existence of considerable amount of such bonds in this particular glass. In this way, the presence of chemical disorder at high pressures is found to be compatible with present double-edge EXAFS data.

Refinements including Ge-Ge and Se-Se correlations (model-2) were found to yield improved fits for most of the pressure points, with residual values 2 to 3 times smaller as compared to the results of model-1 (especially in the 20 to 100 GPa range, see *SI Appendix*, Fig. S3). The Ge-Ge and Se-Se signals are not significant at pressures smaller than 20 GPa, due mainly to reduced CNs. Differences of the residual values of two different fitting procedures have been found to be negligible above 120 GPa because of the limited *k*-range and increased noise of the EXAFS signals. Nevertheless, we used model-2 also for the data above 100 GPa, in order to obtain consistent results. The k^2 weighted experimental and corresponding best-fit theoretical EXAFS signals of all pressure points were plotted in *SI Appendix*, Fig. S4. We can see that highly satisfactory EXAFS refinements could be achieved for the entire pressure range of the present study.

Thanks to the strong constraints on the parameters space imposed by the double-edge refinements, quantitative information beyond the first shell Ge-Se distributions could be obtained from present EXAFS investigation for a wide pressure range up to 157 GPa. The introduction of three different correlations (Ge-Se, Ge-Ge, and Se-Se) was done taking care of the number of floating parameters and to the possible correlations among them. In particular, the bond variances and CNs are known to be highly correlated. For this reason, the range used to float the coordination numbers was based on MD simulations under high-pressure conditions also indicating an increase of coordination in a range of distances up to 2.9 Å at extremely high pressures as shown in *SI Appendix*, Fig. S5.

Best fit parameters, including average distances *R*, variances σ^2 and CNs of each distance distribution (Ge-Se, Ge-Ge and Se-Se), are plotted as function of pressure in Fig. 4. Interestingly, the evolution of the structural parameters, especially those related to the first neighbor Ge-Se distribution [Fig. 4 *A*–*C*] show some anomalies at similar characteristic pressures where the shift of edge energies have shown distinct trends (Fig. 2). Undoubtedly, this behavior indicates the strong correlation between electronic and structural properties in $GeSe_2$ glass under high pressure. In the following, we will discuss the evolution of best-fit structural parameters step by step, identifying four different stages in the compression process, as indicated by background colors in Fig. 4.

(I): During the initial compression stage up to ~ 11 GPa, the LDA structure is preserved. CN of the first neighbor Ge-Se distribution is roughly constant around its initial values (~4), while the Ge-Se distance (R_{GeSe}) exhibits a rapid decrease and the disorder parameter σ^2_{GeSe} slightly increases. This is a strong indication of the compressed but preserved tetrahedral local ordering. Structural parameters related to Ge-Ge and Se-Se correlations [Fig. 4 *D*–*F*] do not show notable changes. Stability of the LDA phase is consistent with the nearly constant edge energies within this pressure range (Fig. 2). As discussed early, changes at the medium range including the conversion from edge-sharing to corner-sharing tetrahedral configurations, are reflected in the evolution of the XANES features (Fig. 1 *A* and *B*).

(II): The second compression stage within 11 to 30 GPa is a transitional stage from LDA to HDA form. Trend of the R_{GeSe} is reversed above 11 GPa, showing a rapid elongation reaching to a maximum value of about 2.4 Å at 30 GPa. Such a behavior is usually regarded as an important signature of the transition toward the HDA phase, often accompanied by an increase in CNs (1, 5–7, 17, 25). Indeed, as expected, best fit first neighbor CNs [CN_{GeSe}, see Fig. 4*C*] also show rapid increase within this pressure range. Elongation of the average distance R_{GeSe} under pressure here is a reasonable behavior due to the fact that the average distance needs to be larger to accommodate more atoms within the first shell of neighbors. In addition, variances parameter σ^2_{GeSe} also shows a simultaneous increase along with

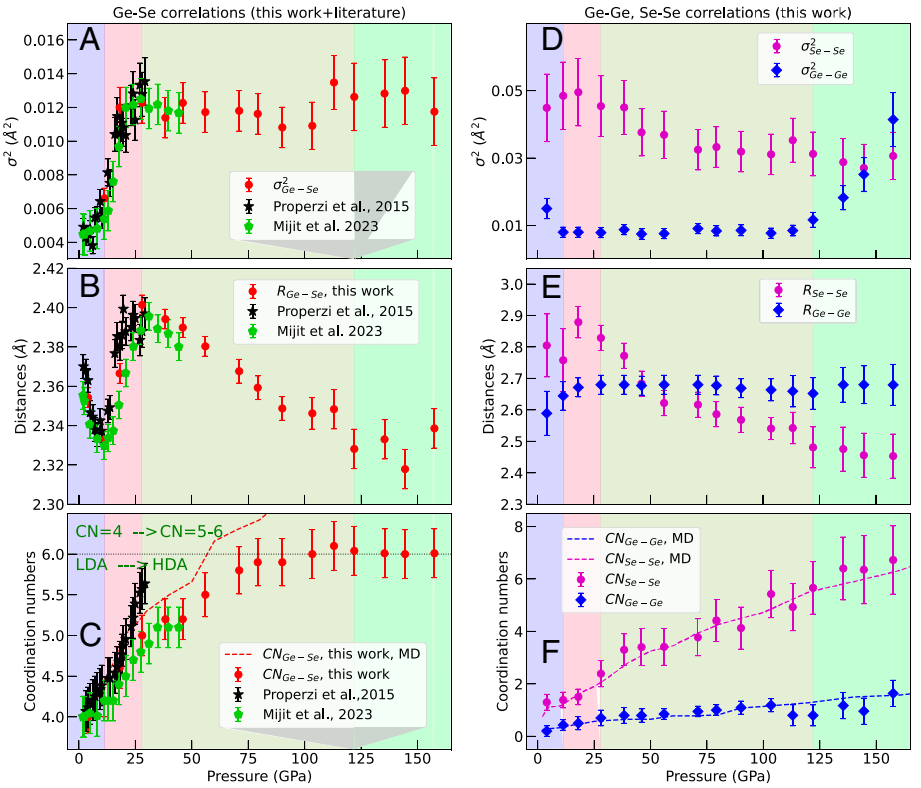

Fig. 4. Pressure evolution of the structural parameters measured by XAS in this work, compared with previous determinations and present MD results. The panels on the *Left* side show the parameters of the Ge-Se distribution: disorder parameters (*A*), atomic distances (*B*), and coordination (*C*). The *Right*-hand panels report the parameters related to the homopolar Ge-Ge and Se-Se distributions: disorder parameters (*D*), atomic distances (*E*), and coordination numbers (*F*).

R_{GeSe} and CN_{GeSe}, reflecting the dramatic increase of the disorder within the glass. This is a consequence of the breakdown of the homogeneous fourfold tetrahedral coordination into more chaotic local configurations, characterized by a mixture of various species with different CNs (four, five, and six-fold). Variations in the parameters related to Ge-Ge and Se-Se correlations remain negligible, with only slight increases observed in R_{SeSe} and CN_{SeSe}.

(III): In the third compression stage, spanning from 30 to 120 GPa, the HDA phase becomes stabilized and undergoes further compression. Therefore, above 30 GPa the behavior of R_{GeSe} is found to change again, reversing from the increasing trend to the decreasing one. The average distance R_{GeSe} continuously decreases from its peak value (∼2.40 Å, at $P \approx 30$ GPa) to a value of about ∼2.32 Å at 120 GPa. Average CNs of nearest neighbor Ge−Se distribution is also increased from ∼5.0 to ∼6.0, but with a slower rate. Meanwhile, the variances σ^2_{GeSe} remains relatively stable around its maximum value (∼0.012 Å^{-2}), within the range of estimated error bars. The observed second decreasing trend of R_{GeSe} is a typical signature of entrance to the HDA state. However, the average CN at the onset pressure (∼30 GPa) is found to be ∼5.0, instead of 6.0 expected for the HDA phase. This suggests that the glass structure at the onset pressure is composed of a mixture of 4, 5, and 6 fold coordinated units, and the fraction of the 6-fold species will rapidly increase and become dominant upon further compression. Nevertheless, the saturation of σ^2_{GeSe} and gradual shortening of the atomic distance R_{GeSe} indicate the dominance of HDA component in the glass above 30 GPa. Interestingly, the Se-Se CNs increase clearly while average Se-Se distances decrease with pressure. This indicates a closer arrangement of Se atoms, leading to the formation of Se-Se bonds and chains or ring-like structures. This observation is consistent with molecular dynamics (MD) simulations conducted in previous studies (7) and the present work (*SI Appendix*). The formation of Se-Se bonds and the enhanced Se-Se correlations are consistent with the gradual increase in the Se K-edge energy reported earlier in Fig. 2, due to the fact that growing population of Se-Se bonds increases average effective valence of Se.

(IV): During the final compression state from 120 to 160 GPa, the CN_{GeSe} reaches a plateau, stabilizing at the average value of the octahedral coordination $CN_{GeSe} \sim 6$, while the number of "wrong" bonds monitored by CN_{SeSe} and CN_{GeGe} is still increasing. The Ge-Se distance R_{GeSe} fluctuates around a value of ∼2.33 Å, also suggesting a saturating trend, while there is a reduction of R_{SeSe} and a stabilization of the R_{GeGe} average distances. On the other hand, there is a slight increase in the disorder parameter σ^2_{GeSe}, indicating a growing level of disorder within the system at extreme pressures. A notable observation is the rapid and significant increase of the disorder parameter σ^2_{GeGe}. To conclude, during this compression stage, the HDA phase related to the octahedral Ge-Se coordination is found to be stable but there is an indication of a further evolution to a new higher-density amorphous phase. However, further experiments exploring higher pressure ranges are necessary to confirm the existence of a potential second higher-density amorphous form.

Conclusions

Pressure-induced polyamorphism has been studied in $GeSe_2$ glass under ultrahigh-pressure conditions up to 157 GPa. We used state-of-the-art double-edge XAS analysis assisted by MD simulations. The evolution of the X-ray absorption near-edge

structures related also to the peculiar semiconductor-metal transition in this disordered system has been observed in the full range of pressures, showing a 2 eV red shift of the Ge K-edge and a slight (0.5 eV) blue shift of the Se K-edge at ultrahigh pressures (above 100 GPa). Thanks to the quality of the XAS data, we were able to perform a detailed analysis of the structure evolution including the presence of short-range chemical disorder, using accurate EXAFS refinements and MD simulations. It is shown that the LDA-HDA transition from tetrahedral to octahedral coordination of the Ge sites is completed above $\sim$ 80 GPa, while the number of short Ge-Ge and Se-Se "wrong" homopolar bonds increases upon pressurization. Present findings have been confirmed by our MD simulations also indicating an increase of chemical disorder at high pressure. At ultrahigh pressures, the increase of the Se-Se correlations or the formation of Se cluster of chains within the glass network is compatible also with the observed gradual blue shift of Se K-edge energy, due to the increased average valence of Se resulted from the increased population of Se-Se bonds. Such an information was never obtained experimentally for any glass, especially by means of a direct, element-specific local structural probe. In this work, no direct evidence of a new HDA phase with $CN_{GeSe} > 6$ was found up to the present limiting pressure. The observed trend of structural parameters (e.g., σ^2_{GeSe} and R_{GeSe}) above 120 GPa may indicate an onset of another high-density amorphous phase, but needs to be confirmed by further investigations beyond the pressure limits of this study.

Amorphous-amorphous transformations (AATs, referring to the conversion of the glass structure to a higher density form with distinct local structure in this context) are often considered as thermodynamically linked to an underlying first-order liquid–liquid transition (LLT) within the supercooled liquid state. There are substantial pieces of evidence now that indicate a close connection between AAT and LLT in typical systems like Si, Ge, and water (8–10, 12). However, applying this framework to $GeSe_2$ glass requires systematic theoretical and experimental studies of the liquid phase, particularly in the supercooled regime. Thus, discussing the nature of the observed signatures of AAT in $GeSe_2$ glass is beyond the scope of this manuscript. Nonetheless, the data presented here offer some insights for understanding the pressure behavior of network structures in this and similar glasses (with chemical disorder) in a wide pressure range. Here, using a direct element specific local structural probe assisted by MD simulations, we demonstrate and confirm that the chemical disorder and further formation of Se-Se/Ge-Ge homopolar bonds play an important role for the ultrahigh-pressure behavior of the $GeSe_2$ glass. Even though the $GeSe_2$ glass shows some differences compared to other archetypal oxide glasses (7, 31), and not all the observations in this particular system can be generalized, current study will have important implications for discussing the pressure response of the local atomic and electronic structures in simple tetrahedral network forming glasses under ultrahigh pressures beyond 1 Mbar.

Materials and Methods

Samples. Amorphous $GeSe_2$ samples used in this study were purchased from Sigma-Aldrich (CAS number 12065-11-1, 99.999% purity).

High-Pressure Experiments. Powders of $GeSe_2$ glass have been compressed using membrane-driven diamond anvil cell (DAC) up to 157 GPa. DAC was equipped with nanopolycrystalline diamond (NPD) anvils (with 150 μm culet size)(48, 49) in order to obtain glitch-free EXAFS spectra. A 200 μm thick rhenium gasket was preindented to a final thickness of $\sim$ 30 μm (a value of compromise to have reasonable edge jump for both Ge and Se edges) and laser drilled to obtain a sample chamber of about $\sim$ 75 μm diameter. The sample chamber was filled entirely with amorphous $GeSe_2$ powders, without any pressure transmitting medium (PTM) but with a small piece of gold (Au) for pressure calibrations (50). Pressure measurements using standard ruby fluorescence technique have been avoided during entire experimental procedures for preventing the possible laser-induced crystallization. Before each measurement, pressure was stabilized of about 15 min. Pressure values mentioned in this text are the average of pressure values measured before and after each data point. Performing this experiment without PTM was driven by several considerations. First of all, high-pressure EXAFS experiments with NPD anvils are not compatible with optimal PTMs like He gas, as He easily penetrates into the microstructures of the NPD anvil. Neon (Ne) is sometimes used as a PTM for HP EXAFS experiments with NPD anvils, but from our experiences, there is always some risk of premature failure due to possible Ne penetration depending on the quality of NPD anvils. We therefore avoided using Ne as PTM to reach the maximum pressure possible with the available smallest culet size (150 um) diamonds. Use of liquid PTMs would complicate the sample loading and would not be very useful at very high pressure since hydrostatic pressure limits of liquid PTMs are generally not very high. On the other hand, effects of pressure in-homogeneity are generally believed to be less important for glassy systems. Note that absolute majority of previous ultrahigh-pressure experiments on covalent network forming glasses were commonly performed without any PTM (1, 2, 14, 15, 17, 19, 25). Nevertheless, we have performed an independent run with Ne PTM up to 45 GPa to assess possible differences induced by nonhydrostatic compression. Results from two runs (with and without PTM) show similar pressure behavior (see ref. 29), confirming that there is no considerable negative effect from nonhydrostatic compression.

XAS Measurements. Combined XAS and XRD have been measured under pressure at the BM23 beamline of the European Synchrotron Radiation Facility (ESRF, France) (51). A double crystal monochromator equipped with two Si(111) crystals in fixed exit geometry was employed for monochromatizing the incoming beam. The X-ray beam was focused down to 3×3 μm^2 using two Pt-coated mirrors inclined to 4.0 mrad in Kirkpatrick-Baez (KB) geometry that served also as harmonic rejection mirrors. XRD data have been collected using a Pilatus 1M detector by fixing the monochromator energy at 18.0 keV (0.6888 Å). The sample to detector distance, detector tilt, and incident beam position were calibrated using a cerium oxide powder standard. Calibration of the Pilatus 1M detector and also the integration of two-dimensional images into the one-dimensional XRD patterns have been performed using the software Dioptas (52). XAS data have been measured in transmission mode (in axial geometry through the diamond anvils) scanning through both Ge and Se K-edges at the same pressure points. Reference spectra of a $GeSe_2$ glass pellet at ambient conditions have been also simultaneously measured for each XAS data for the edge energy calibrations.

Molecular Dynamics Simulations. Complementary molecular dynamics simulations were performed using the first-principles pseudopotential method within the density-functional theory (DFT). The exchange correlation term was computed using a generalized gradient approximation (GGA) (53, 54). The norm-conserving Troullier–Martins pseudopotentials (55) were used. The calculations were achieved by the SIESTA ab initio program (56). Double-ζ basis sets were selected for the simulations. The supercell's Brillouin zone integration was done at $\Gamma - k$ point. The calculations were accomplished by means of the isoenthalpic-isobaric ensemble (constant atom, enthalpy, and pressure). The optimization of the atomic structure and supercell's volume at each pressure was accomplished by means of the Parrinello–Rahman (57) and the power quenching (PQ) methods. In the PQ algorithm, the velocities of atoms and supercell's lattice parameters are set to be zero whenever the velocities and forces reserve their signs. For the optimization, the force and stress criteria were set to be 0.01 eV/Å and 0.5 GPa, respectively. The initial amorphous model having 150 atoms was due to Drabold's group and generated using the VASP code (58) within the PBE-GGA (59) exchange-correlation functional. Some structural investigations were performed using the ISAACS program (60)

Data, Materials, and Software Availability. Experimental raw data (x-ray absorption spectroscopy and x-ray diffraction) have been deposited in European

Synchrotron Radiation Facility database (61). All analyzed data are reported in the manuscript and/or *SI Appendix*.

ACKNOWLEDGMENTS. We acknowledge the European Synchrotron Radiation Facility for provision of synchrotron radiation facilities (proposal No: HC-4645). We would like to warmly thank J. Jacobs for his help with the preparation of the diamond anvil cells. E.M. thanks for the "GO FOR IT" postdoc grant from the CRUI (Conferenza dei Rettori delle Università Italiane) foundation.

Author affiliations: [a]Physics Division, School of Science and Technology, University of Camerino, Camerino I-62032, Italy; [b]European Synchrotron Radiation Facility, Grenoble Cedex 9 38043, France; [c]Department of Nanotechnology Engineering, Abdullah Gül University, Kayseri 38080, Turkey; and [d]Geodynamics Research Center, Ehime University, Matsuyama 790-8577, Japan

1. M. Murakami, J. D. Bass, Spectroscopic evidence for ultrahigh-pressure polymorphism in SiO_2 glass. *Phys. Rev. Lett.* **104**, 025504 (2010).
2. Y. Kono, Y. Shu, C. Kenney-Benson, Y. Wang, G. Shen, Structural evolution of SiO_2 glass with Si coordination number greater than 6. *Phys. Rev. Lett.* **125**, 205701 (2020).
3. G. Fiquet *et al*., Melting of peridotite to 140 gigapascals. *Science* **329**, 1516–1518 (2010).
4. R. Nomura *et al*., Low core-mantle boundary temperature inferred from the solidus of pyrolite. *Science* **343**, 522–525 (2014).
5. C. Meade, R. J. Hemley, H. Mao, High-pressure X-ray diffraction of SiO_2 glass. *Phys. Rev. Lett.* **69**, 1387 (1992).
6. J. P. Itie *et al*., Pressure-induced coordination changes in crystalline and vitreous GeO_2. *Phys. Rev. Lett.* **63**, 398–401 (1989).
7. M. Durandurdu, D. A. Drabold, Simulation of pressure-induced polyamorphism in a chalcogenide glass $GeSe_2$. *Phys. Rev. B* **65**, 104208 (2002).
8. P. F. McMillan, Polyamorphic transformations in liquids and glasses. *J. Mater. Chem.* **14**, 1506–1512 (2004).
9. O. Mishima, H. E. Stanley, The relationship between liquid, supercooled and glassy water. *Nature* **396**, 329–335 (1998).
10. P. F. McMillan, M. Wilson, D. Daisenberger, D. Machon, A density-driven phase transition between semiconducting and metallic polyamorphs of silicon. *Nat. Mater.* **4**, 680–684 (2005).
11. L. Properzi, A. Di Cicco, L. Nataf, F. Baudelet, T. Irifune, Short-range order of compressed amorphous $GeSe_2$. *Sci. Rep.* **5**, 1–9 (2015).
12. E. Principi *et al*., Polyamorphic transition of germanium under pressure. *Phys. Rev. B* **69**, 201201 (2004).
13. A. Zeidler, P. S. Salmon, L. B. Skinner, Packing and the structural transformations in liquid and amorphous oxides from ambient to extreme conditions. *Proc. Natl. Acad. Sci. U.S.A.* **111**, 10045–10048 (2014).
14. Y. Kono *et al*., Ultrahigh-pressure polyamorphism in GeO_2 glass with coordination number > 6. *Proc. Natl. Acad. Sci. U.S.A.* **113**, 3436–3441 (2016).
15. C. Prescher *et al*., Beyond sixfold coordinated si in SiO_2 glass at ultrahigh pressures. *Proc. Natl. Acad. Sci. U.S.A.* **114**, 10041–10046 (2017).
16. S. K. Lee *et al*., Oxygen quadclusters in SiO_2 glass above megabar pressures up to 160 GPa revealed by X-ray Raman scattering. *Phys. Rev. Lett.* **123**, 235701 (2019).
17. T. Sato, N. Funamori, High-pressure structural transformation of SiO_2 glass up to 100 GPa. *Phys. Rev. B* **82**, 184102 (2010).
18. S. Petitgirard *et al*., Magma properties at deep earth's conditions from electronic structure of silica. *Geochem. Perspect. Lett* **9**, 32–37 (2019).
19. G. Spiekermann *et al*., Persistent octahedral coordination in amorphous GeO_2 up to 100 GPa by K_β X-ray emission spectroscopy. *Phys. Rev. X* **9**, 011025 (2019).
20. Y. H. Kim *et al*., Pressure-driven changes in the electronic bonding environment of GeO_2 glass above megabar pressures. *J. Am. Chem. Soc.* **144**, 10025–10033 (2022).
21. M. Vaccari *et al*., Structural changes in amorphous GeS_2 at high pressure. *Phys. Rev. B* **81**, 014205 (2010).
22. C. Yildirim *et al*., Universal amorphous-amorphous transition in Ge_xSe_{100-x} glasses under pressure. *Sci. Rep.* **6**, 27317 (2016).
23. L. Properzi *et al*., Structural evolution mechanisms of amorphous and liquid As_2Se_3 at high pressures. *Phys. Rev. B* **93**, 214205 (2016).
24. A. Di Cicco, X-ray absorption spectroscopy investigations of disordered matter. *Radia. Phys. Chem.* **175**, 108077 (2020).
25. M. Krstulović *et al*., Ge coordination in $NaAlGe_3O_8$ glass upon compression to 131 GPa. *Phys. Rev. B* **101**, 214103 (2020).
26. M. Krstulović, A. D. Rosa, N. Biedermann, T. Irifune, M. Wilke, Structural changes in aluminosilicate glasses up to 164 GPa and the role of alkali, alkaline earth cations and alumina in the densification mechanism. *Chem. Geol.* **560**, 119980 (2021).
27. K. Wezka *et al*., Density-driven defect-mediated network collapse of $GeSe_2$ glass. *Phys. Rev. B* **90**, 054206 (2014).
28. E. Soignard *et al*., Pressure-driven chemical disorder in glassy mAs_2S_3 up to 14.7 GPa, post-densification effects, and applications in materials design. *J. Phys. Chem. B* **124**, 430–442 (2019).
29. E. Mijit *et al*., EXAFS investigations on the pressure induced local structural changes of $mGeSe_2$ glass under different hydrostatic conditions. *J. Phys.: Condens. Matter* **35**, 264001 (2023).
30. I. Petri, P. S. Salmon, H. E. Fischer, Defects in a disordered world: The structure of glassy $GeSe_2$. *Phys. Rev. Lett.* **84**, 2413–2416 (2000).
31. P. S. Salmon, I. Petri, Structure of glassy and liquid $mGeSe_2$. *J. Phys.: Condens. Matter* **15**, S1509 (2003).
32. Z. Y. Wu *et al*., Characterization of iron oxides by X-ray absorption at the oxygen K edge using a full multiple-scattering approach. *Phys. Rev. B* **55**, 2570–2577 (1997).
33. S. F. Mayer *et al*., A comprehensive examination of the local-and long-range structure of Sb_6O_{13} pyrochlore oxide. *Sci. Rep.* **10**, 1–14 (2020).
34. E. Mijit, K. Chen, F. Choueikani, A. Di Cicco, F. Baudelet, Collapse of itinerant ferromagnetism in CoS_2 under pressure: An X-ray absorption spectroscopy study. *Phys. Rev. B* **98**, 184423 (2018).
35. E. Mijit *et al*., Crystal and electronic structure of Co_3O_4 spinel under pressure probed by Xanes and Raman spectroscopy. *Phys. Rev. B* **103**, 024105 (2021).
36. P. Krüger, "Electronic structure theory for X-ray absorption and photoemission spectroscopy" in *Magnetism and Accelerator-Based Light Sources*, H. Bulou, L. Joly, J. M. Mariot, F. Scheurer, Eds. (Springer International Publishing, Cham, 2021), pp. 63–81.
37. Q. Mei *et al*., Topological changes in glassy $mGeSe_2$ at pressures up to 9.3*m*GPa determined by high-energy X-ray and neutron diffraction measurements. *Phys. Rev. B* **74**, 014203 (2006).
38. F. Wang, S. Mamedov, P. Boolchand, B. Goodman, M. Chandrasekhar, Pressure Raman effects and internal stress in network glasses. *Phys. Rev. B* **71**, 174201 (2005).
39. S. M. Antao *et al*., Network rigidity in $GeSe_2$ glass at high pressure. *Phys. Rev. Lett.* **100**, 115501 (2008).
40. A. Filipponi, A. Di Cicco, Short-range order in crystalline, amorphous, liquid, and supercooled germanium probed by X-ray-absorption spectroscopy. *Phys. Rev. B* **51**, 12322–12336 (1995).
41. A. Di Cicco *et al*., Interplay between morphology and metallization in amorphous-amorphous transitions. *Phys. Rev. B* **78**, 033309 (2008).
42. S. Asokan, M. V. N. Prasad, G. Parthasarathy, E. S. R. Gopal, Mechanical and chemical thresholds in IV-VI chalcogenide glasses. *Phys. Rev. Lett.* **62**, 808–810 (1989).
43. M. Prasad, S. Asokan, G. Parthasarathy, S. Titus, E. Gopal, Electrical resistivity studies on Ge-Se glasses at high pressures and low temperatures. *Phys. Chem. Glass.* **34**, 199–202 (1993).
44. A. Filipponi, A. Di Cicco, C. R. Natoli, X-ray absorption spectroscopy and n-body distribution functions in condensed matter (I): Theory. *Phys. Rev. B* **52**, 15122–15134 (1995).
45. A. Filipponi, A. Di Cicco, X-ray absorption spectroscopy and n-body distribution functions in condensed matter (II): Data-analysis and applications. *Phys. Rev. B* **52**, 15135 (1995).
46. A. Filipponi, A. Di Cicco, GNXAS: A software package for advanced EXAFS multiple-scattering calculations and data-analysis. *TASK Quart.* **4**, 575–669 (2000).
47. A. Di Cicco, Multiple-edge EXAFS refinement: Short-range structure in liquid and crystalline Sn. *Phys. Rev. B* **53**, 6174–6185 (1996).
48. T. Irifune, A. Kurio, S. Sakamoto, T. Inoue, H. Sumiya, Materials: Ultrahard polycrystalline diamond from graphite. *Nature* **421**, 599 (2003).
49. N. Ishimatsu *et al*., Glitch-free X-ray absorption spectrum under high pressure obtained using nano-polycrystalline diamond anvils. *J. Synch. Radiat.* **19**, 768–772 (2012).
50. Y. Fei *et al*., Toward an internally consistent pressure scale. *Proc. Natl. Acad. Sci. U.S.A.* **104**, 9182–9186 (2007).
51. O. Mathon *et al*., The time-resolved and extreme conditions XAS (TEXAS) facility at the European synchrotron radiation facility: The general-purpose EXAFS bending-magnet beamline BM23. *J. Synchr. Radia.* **22**, 1548–1554 (2015).
52. C. Prescher, V. B. Prakapenka, DIOPTAS: A program for reduction of two-dimensional X-ray diffraction data and data exploration. *High Press. Res.* **35**, 223–230 (2015).
53. A. D. Becke, Density-functional exchange-energy approximation with correct asymptotic behavior. *Phys. Rev. A* **38**, 3098–3100 (1988).
54. C. Lee, W. Yang, R. G. Parr, Development of the Colle-Salvetti correlation-energy formula into a functional of the electron density. *Phys. Rev. B* **37**, 785 (1988).
55. N. Troullier, J. L. Martins, Efficient pseudopotentials for plane-wave calculations. *Phys. Rev. B* **43**, 1993 (1991).
56. J. M. Soler *et al*., The SIESTA method for ab initio order-N materials simulation. *J. Phys.: Condens. Matter* **14**, 2745 (2002).
57. M. Parrinello, A. Rahman, Polymorphic transitions in single crystals: A new molecular dynamics method. *J. Appl. Phys.* **52**, 7182–7190 (1981).
58. G. Kresse, J. Furthmüller, Efficient iterative schemes for ab initio total-energy calculations using a plane-wave basis set. *Phys. Rev. B* **54**, 11169 (1996).
59. J. P. Perdew, K. Burke, M. Ernzerhof, Generalized gradient approximation made simple. *Phys. Rev. Lett.* **77**, 3865 (1996).
60. S. Le Roux, V. Petkov, ISAACS-interactive structure analysis of amorphous and crystalline systems. *J. Appl. Crystall.* **43**, 181–185 (2010).
61. Y. Mijiti *et al*., From "Investigation of the local structural changes in $GeSe_2$ glass under ultrahigh pressure". European Synchrotron Radiation Facility. https://doi.org/10.15151/ESRF-ES-551397497. Deposited 3 November 2021.